Micron 41 (2010) 135–142

Contents lists available at ScienceDirect

Micron

journal homepage: www.elsevier.com/locate/micron

Quantitative HRTEM investigation of nanoplatelets

Frédéric Pailloux *, Marie-Laure David, Laurent Pizzagalli

Laboratoire de Physique des Matériaux, UMR6630 CNRS-Université de Poitiers, SP2MI, Bd M. et P. Curie, BP 30179, 86962 FUTUROSCOPE-CHASSENEUIL, France

ARTICLE INFO

Article history:
Received 29 June 2009
Received in revised form 17 September 2009
Accepted 17 September 2009

PACS:
68.37.Og
61.72.−y
31.15.A
81.05.Cy

Keywords:
HRTEM
Image analysis
Image simulation
Crystal defects

ABSTRACT

High resolution transmission electron microscopy experiments were performed to investigate nanoplatelets induced by ion implantation into a germanium wafer. Atomistic models were used for image simulation in order to get quantitative information from the experimental images. The geometrical phase shift analysis technique was also employed to measure the strain field induced by such defects. We discuss the limits and artefacts imposed by each approach and show how these approaches can be combined to study the atomic structure of such defects and the strain field they induce.

1. Introduction

The term "Platelets" is commonly used in the literature to denote two-dimensional defects. Platelets are encountered in diamond-type structure and structures derived from it: sphalerite and wurtzite. Their presence was reported since the early 60s and extensively studied in diamond (Evans and Phaal, 1962; Barry, 1991). In other covalent crystals such as Si, Ge, GaAs, InP or GaN platelets can be created by a high dose incorporation of hydrogen or helium into a wafer via implantation or diffusion (Terreault, 2007; Fichtner et al., 1999; David et al., 2007; Nomachi et al., 1997; Hayashi et al., 2004; Moutanabbir et al., 2008). Helium platelets have also been widely studied in metals, in the framework of nuclear applications (Evans et al., 1981). In all cases, these defects are at the origin of strong surface or sub-surface modifications (blistering, exfoliation, layer splitting) that triggered out a huge amount of studies for materials improvement in the field of nuclear technology and for defect engineering in semiconductors.

The questions related to platelet description concern the geometrical parameters (width and lateral extent), the composition (presence of vacancies, interstitials or impurities) and the lattice displacement they induce. Whatever the system, direct experimental methods are required to give an accurate description of the atomic structure of the platelets. Their analysis is a long-standing and challenging problem for transmission electron microscopy (TEM), closely related to the analysis of Guinier–Preston zones in CuAl alloys.

Since the pioneer works from Evans and Phaal (1962) in type I diamond, many TEM approaches were employed to measure the strain field surrounding platelets and to probe their atomic structure. The estimation of the strain field was mainly conducted by using a Moiré fringe technique (Bursill et al., 1981) or based on the refinement of the intensity in images obtained under two-beam conditions (Humble, 1982; Muto et al., 1995). Measurements were also performed by large angle convergent beam electron diffraction on large platelets (Cherns et al., 1997). Naturally, the determination of their atomic structure was tackled by matching the experimental HRTEM contrast with simulated images (Barry, 1991; Bursill et al., 1978; Humble et al., 1985), with various levels of accuracy depending on the performances of the microscopes used and on the level of discrepancy between the atomic models to be discriminated. These last experiments were mainly performed on relatively large platelets (viewed edge-on) to ensure that they thread the electron microscopy sample, in order to compare experimental and simulated contrasts.

The level of knowledge concerning the structure of hydrogen-induced platelets (HIPs) in semiconductor can be summarized by the following assessment: the determination of the strain field and

* Corresponding author.
E-mail address: frederic.pailloux@univ-poitiers.fr (F. Pailloux).

0968-4328/$ – see front matter © 2009 Elsevier Ltd. All rights reserved.
doi:10.1016/j.micron.2009.09.005

atomic structure of platelets have never been performed on the same defects. Indeed, the strain field measurements were mostly obtained for embedded platelets whereas the atomic structure refinements were extracted from platelets from which edges were cut (so that they thread the sample) (Neethling et al., 1988). This point could be considered as minor detail, but if one considers that strain relaxation occurs during the specimen preparation (especially by releasing the stress at edges), then one can easily admit that the images would be affected by removing the edges of a defect. The situation becomes critical in the case of gas-filled defect from which the possible trapped gas would have been released by cutting the edges. This is a pitfall in the understanding of the nucleation and evolution of these defects, as the two approaches reported above can hardly be compared. Bringing together strain field measurements, atomic structure refinement and results obtained from theoretical calculations is expected to be very fruitful. Such an approach has recently allowed establishing that platelets in diamond were related to the presence of nitrogen (Goss et al., 2003).

In the case of nanometric HIPs (nanoplatelets), as a consequence of the scale of investigation, HRTEM is the only relevant approach. An elegant and accurate method for evaluating the displacement field around defects in crystals from HRTEM images was proposed by Hÿtch et al. (1998). This geometrical phase shift analysis (GPA) method was successfully employed to measure displacement field around dislocations in silicon with accuracy better than 0.003 nm (Hÿtch et al., 2003). Recently, an attempt to measure the displacement field around nanoplatelets, produced by boron implantation in silicon, by a combination of weak-beam dark field imaging and GPA analysis was reported (Cherkashin et al., 2005). However the authors did not mention whether the defects studied by HRTEM were embedded in the thin electron microscopy sample or not, which is a critical point for HRTEM image interpretation. Moreover, in the case of gas-filled cavities, as the strain field along the electron beam path is inhomogeneous, the contrast variations with observation conditions (crystal thickness, defocus, ...) might be unpredictable (Cherns et al., 1997; Spence, 1982). Otherwise speaking, one cannot assess that the atomic columns coincide with white (or black) dots in the whole image, especially close to the core of the defect, where the displacement field could be relatively high. Such effects could notably distort the results given by the GPA method. Thus, probing the exact stoichiometry and the atomic structure of nanoplatelets from quantitative HRTEM experiments seems to remain challenging.

It appears essential in such a case to combine image simulation based on atomistic models with the GPA method. In this paper we discuss the limits and artefacts of such an approach applied to embedded defects. We finally show that the combination of the HRTEM contrast matching, displacement field analysis via the GPA method and DFT calculation leads to a reasonable description of the structure of nanoplatelets and their associated strain field.

2. Technical details

HIPs were obtained by high fluence hydrogen implantation in a n-type (0 0 1) germanium wafer (details are given in David et al., 2007). HRTEM experiments were performed in the cross-section geometry along the [1 $\bar{1}$ 0] zone axis. The TEM sample was mechanically polished with a tripod polisher down to 10 μm and subsequently thinned by ion milling in a GATAN-PIPS apparatus until electron transparency. Low energy (2.5 keV) and low incidence (±8° and ±6° for the final step) were used to minimize irradiation damage. This procedure ensures the completion of wide thin areas required to perform quantitative HRTEM (Q-HRTEM). HRTEM images were recorded by using a JEOL 3010 operated at 300 kV (LaB_6, C_s = 1.2 mm, 0.19 nm point-to-point resolution). Focus series were acquired either on photographic film or with an ORIUS SC 1000 CCD camera at nominal magnifications of 400 and 600 K. Photographic films were further digitized either at 1200 dpi (dot per inch) or 2400 dpi providing an adequate sampling of atomic columns for GPA analysis. Despite the high voltage used for these experiments, we did not observe the formation of irradiation-induced extended defects. HRTEM pictures were then analyzed with the GPA method to estimate the strain field surrounding the platelets. The HRTEM contrast was simulated using the JEMS package (Stadelmann, 1987) in the multislice framework. For all calculations, the Debye-Waller factors were set to 0.005 nm^3 (which is highly questionable for the atoms located at the core of the defect); details can be found in Barbot et al. (2008). Sample thickness t_s and objective defocus Δf were determined by image matching of a strain free region, located several tens of nanometres away from the studied defects, with thickness/defocus maps calculated using both Bloch wave approach and multislice method. Input models for multislice simulations of the contrast of the defects were obtained from atomistic simulations performed with the Tersoff inter-atomic potential (Tersoff, 1989) Different configurations of the core of the platelets were considered: the number of removed Ge-atoms layers was varied as well as the shift δ between the core atoms along the [0 0 1] direction (incremental step was set to 0.01 nm) (David et al., 2009). The atomic positions surrounding the fixed core atoms were then relaxed until atomic forces became negligible. The contrast simulation was then carried out following two main steps: first we considered a defect threading the sample, and afterwards we built a model in which the defect had a finite size t_d along the electron beam path (embedded in a matrix, see Fig. 1). The contrast matching between experiments and simulations was then optimized by varying δ (0.01 nm step), the position h_d and the thickness t_d of the defect (by 0.8 nm steps). Total thickness t_s and objective defocus Δf were also optimized by fine tuning around the values previously determined from a strain free region. Threefold astigmatism influence was deliberately not considered in this study (Merkle et al., 1998), since the lattice fringes imaged here are the same across the image, which would not imply an artificial expansion of the core of the defect (the situation significantly differs from the case of an asymmetric grain boundary). Complementary to this classical approach in Q-HRTEM, the simulated images were also analyzed using the GPA method in order to compare the phase images obtained from experimental micrographs and simulated pictures. These results were finally checked against density functional theory (DFT) calculations; details concerning the latter are given elsewhere (David et al., 2009).

3. HRTEM experiments on nanoplatelets

Fig. 2a shows the deeper part of the buried defect layer produced by H implantation in Ge. (0 0 1) platelets which sizes range from 5 to 10 nm are observed. On this picture, it is worth

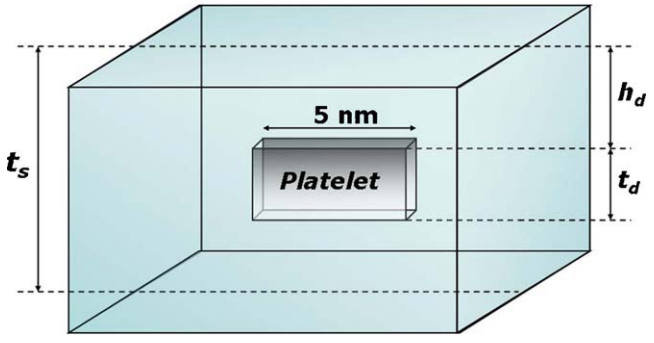

Fig. 1. Sketch of a nanoplatelet embedded in a TEM sample depicting the geometrical parameters used for our calculations.

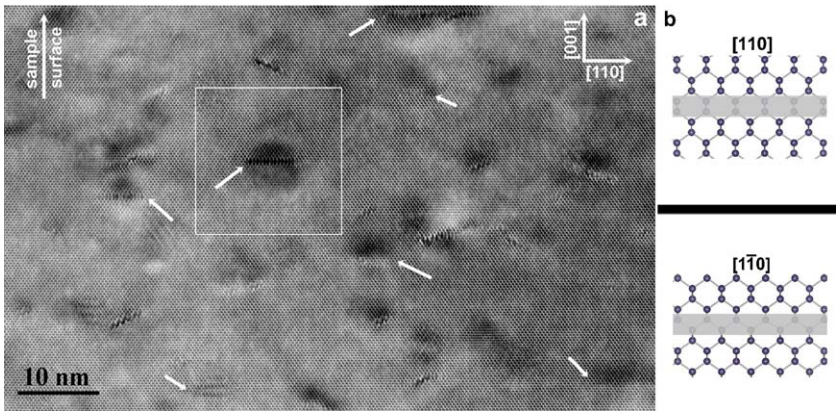

Fig. 2. (a) Overview of the deeper part of the defect layer produced by H implantation in Ge (5×10^{16} cm^{-2}, 15 keV, RT). Some (0 0 1) nanoplatelets are indicated by arrows (other inclined defects are {1 1 3} defects). (b) Sketches of the [1 1 0] (top) and [1 $\bar{1}$ 0] (bottom) projections showing the asymmetry when 2 adjacent Ge rows are removed (grey region) from the core of the defect.

noticing that although the thickness is rather homogeneous over the field of view, the (0 0 1) nanoplatelets give rise to slightly different contrasts without any correlation with their size. These contrast variations could come from the fact that [1 1 0] and [1 $\bar{1}$ 0] directions might not be equivalent for a given defect (see Fig. 2b). Actually if one considers a defect in which 2 Ge rows have been removed from its core, then the [1 1 0] and [1 $\bar{1}$ 0] directions look different. Other origins of these contrast variations will be discussed afterwards.

In order to determine the atomic structure of (0 0 1) nanoplatelets and their associated displacement field, we had to find a defect isolated enough from other defects so that its contrast would not be affected by a disruptive strain field. The platelet in the middle of Fig. 2 (see Fig. 3a) fulfils this requirement and seems thus suitable for GPA. The corresponding diffractogram is displayed in Fig. 3b; a diffuse streak induced by the periodicity breakdown caused by the defect clearly extends between the $\langle 1\,1\,1 \rangle^*$ spots and from the central spot toward the [0 0 2]* direction. Different lattice fringes can be considered to apply the GPA method: either the {1 1 1} or the (0 0 2) and (2 2 0). Slight differences (not shown here) between the two approaches are observed: they are likely due to the fact that {1 1 1}, (0 0 2) and (2 2 0) fringes are differently affected by the contrast transfer function (CTF) during the image formation process in the microscope. Despite these discrepancies, both results confirm that the induced strain field is mainly oriented along the [0 0 1] direction and is almost null in the perpendicular one. The phase shift image for the (0 0 2) fringes is displayed in Fig. 3c; in the case of uniaxial strain field in the [0 0 1] direction, this image contains all the information needed to characterize the displacement field. Moreover in our case, we have noticed that the noise level in this (0 0 2) phase shift image is weaker than that in the strain maps obtained by a combination of {1 1 1} phase images.

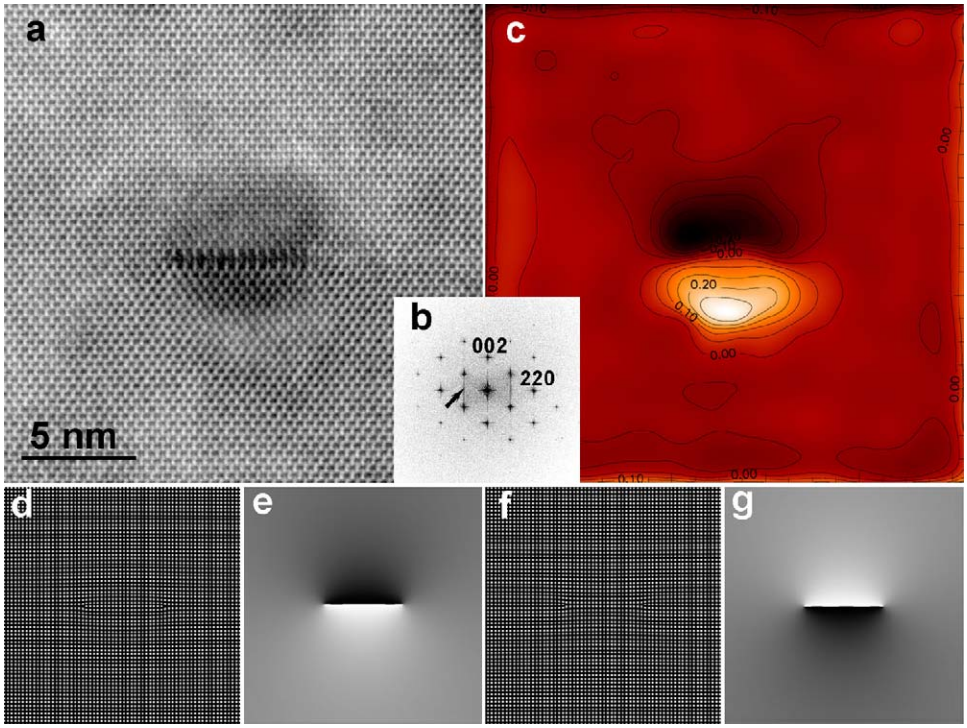

Fig. 3. (a) Typical HRTEM image of an isolated {0 0 1} platelet. (b) Diffractogram of (a). The arrow indicates the diffuse streak induced by the lattice discontinuity due to the nanoplatelet. (c) Phase shift image obtained from the 0 0 2 reflection. The iso-lattice-shift curves are expressed as a fraction the $d_{0\,0\,2}$ lattice spacing. (d) and (f) Lattice models for respectively, an interstitial dislocation loop and a vacancy loop. (e) and (g) Corresponding (0 0 2) phase shift maps.

In the following, we will thus consider (0 0 2) phase shift images to measure the displacement fields around defects.

To some extent, this phase shift image ($\varphi_{0\,0\,2}$) is similar to the ones obtained from dislocation loops models (Fig. 3e and f). It is divided into two main regions: one half in which the phase shift is positive, the other half exhibiting a negative phase shift. As for the case of an interstitial loop (Fig. 3e), the positive displacements $u_{0\,0\,2}$ (defined by $\varphi_{0\,0\,2} = g_{0\,0\,2} \times u_{0\,0\,2}$) of (0 0 2) fringes are in the lower part of the image. This would indicate that the surrounding lattice experience a compressive strain field, which drops to zero, 10 nm away from the core of the defect. A striking point of this image is that the maximum phase shift (i.e. the maximum lattice shift) is observed few inter-atomic distances away from the core of the platelet. The maximum lattice shift measured on this image is $u_{0\,0\,2} = 0.07$ nm ($0.25 \times d_{0\,0\,2}$ with $a_{Ge} = 0.568$ nm). We point out that the same shift of this maximum is observed in phase images obtained with {1 1 1} lattice fringes and does not depend on the characteristics of the mask used for during the processing. Thus, this peculiar feature cannot be assigned to artefacts exclusively due to information transfer via the CTF. Nevertheless it is physically unlikely to consider that atoms located at the core of the defect could experience a weaker shift than those located in the adjacent planes. In order to elucidate this point we have collected through-focus series for a group of platelets. Two images extracted from a focus series are displayed in Fig. 4, together with their associated (0 0 2) phase shift images. These images obviously show that the amplitudes of the phase shifts (and thus the measured displacement field), for a given defect, depend on the defocus value.

This point has to be linked with the remark we made above concerning the differences in contrast observed in Fig. 2 for different nanoplatelets. It comes out that in the case of embedded defects, with various sizes and positions in the sample along the electron beam path, not even the lattice fringes intensity but also their relative position to the projected atomic column across the image are affected by a subtle combination of effects described in the following. It unambiguously establishes that the interpretation of HRTEM images, and as a consequence, of phase shift images for embedded defects is definitely not as straightforward as for the case of threading defects (dislocation viewed edge-on for instance; Hÿtch et al., 2003). Further investigations are thus required to fully interpret these images. To overcome these difficulties, we propose to combine HRTEM image simulation with the GPA method, as expounded in the next section.

4. HRTEM image simulation and discussion

As we will show in the following, the goal here is twofold: achieving a good match between experimental and simulated contrast and a good agreement between phase images obtained from both experimental micrographs and simulation. Let us consider the nanoplatelet shown in Fig. 3a. In a first step, we aim to determine some imaging parameters by matching the experimental contrast of a strain free region with thickness/defocus maps calculated either with a Bloch wave approach or with the multislice method (Fig. 5). All reflections were included in the Bloch wave calculations (the Bethe approximation was also considered, but the gain in computing time was relatively poor). The super-cell thickness for the mutislice calculations was finally set to 0.802 nm which provides a good match between these two approaches. A good correlation between experimental and simulated contrasts is obtained for a sample thickness t_s ranging

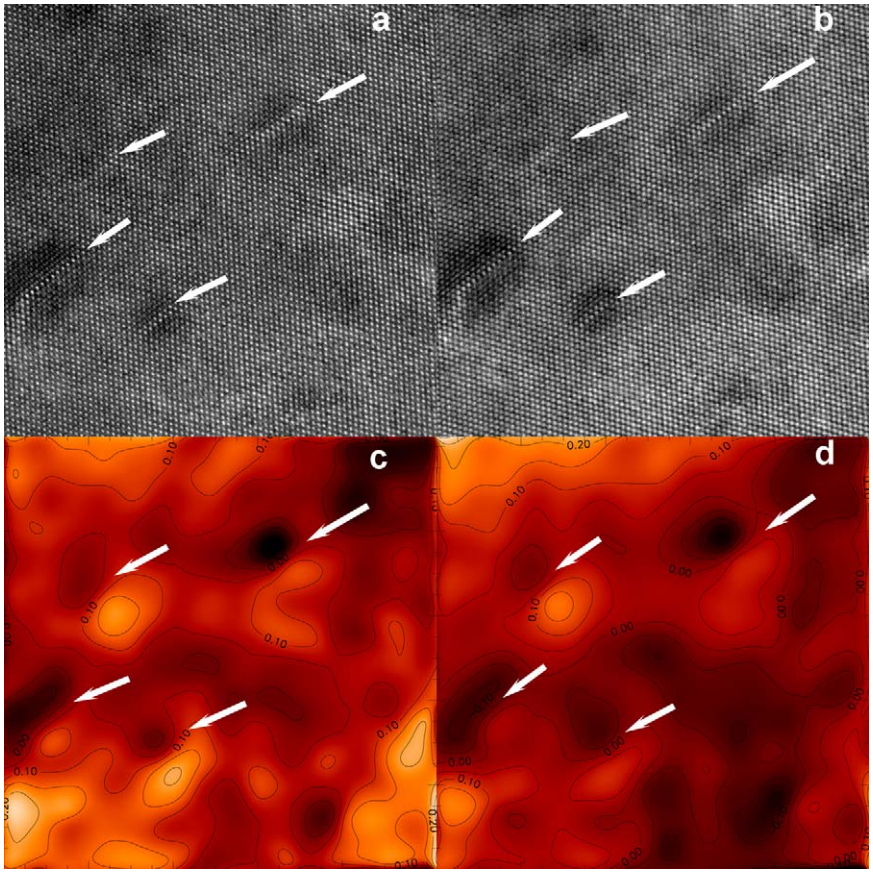

Fig. 4. (a) and (b) HRTEM images of a group of platelets (marked by arrows) extracted from a focus series. (c) and (d) (0 0 2) phase shift images of (a) and (b) showing the influence of the defocus on the measured lattice shift.

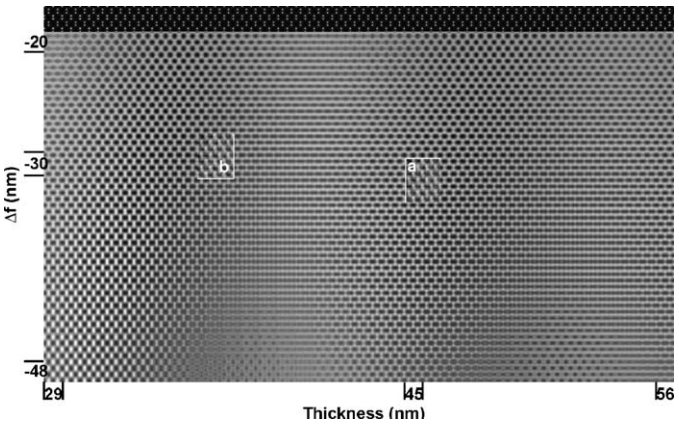

Fig. 5. Thickness/defocus map calculated by the multislice method. Insets (a) and (b), extracted from Fig. 3a, show the good match between the experimental contrast and the simulation. The first row on the top of the image shows the projected atomic potential.

from 44 to 48 nm and for defocus values Δf ranging from −28 to −34 nm (inset of Fig. 5). It is worth noticing that similar levels of agreement can be achieved for other thickness ranges (for instance: 34–38 nm for the same defocus values), but, as experimental pictures were acquired relatively far from the sample surface (i.e. far from the hole drilled during the ion milling, about 200 nm beneath the surface), the previous values seem reasonable. We would like to point out that this dumbbell-like contrast is rather misleading; the atomic columns do not project on the white dots (as seen in Fig. 5), but between (the point resolution of the microscope we use being too low to resolve the atom dumbbells). However, it would not perturb the phase shift images since only spatial frequencies will be analyzed.

Having this fair knowledge of the thickness and defocus ranges corresponding to our experimental conditions, we further focus on the geometrical characteristics of the platelet shown in Fig. 3a: i.e. the dilatation δ at the core of the defect, its position in the sample h_d and its thickness t_d ranging from the smallest size observed in our experiments (4 nm) to t_s. The faulted crystal for multislice calculations was constructed as follow: several slices of perfect Ge crystal were stacked in order to reach a thickness h_d, then, faulted slices were added to produce a defect of thickness t_d and finally, slices of perfect crystal were used to achieve the total thickness t_s (see Fig. 1). The faulted slices were realized by removing two rows having a width of twelve Ge atoms at the centre of the slice. The facing Ge neighbours were then symmetrically and rigidly shifted by δ along the [0 0 1] direction. The system was then relaxed by minimization of atomic forces (David et al., 2009).

Our simulations confirm that the contrast at the core of the platelet cannot be matched to the experimental one by considering a threading defect. The contrast remains strongly bright whatever the defocus values as a consequence of the missing atoms (not shown here), as already reported by other authors (Cherns et al., 1997). Then, a trial and error method was then used to optimize the contrast matching by varying h_d, t_d, δ. It happens that variations of these three parameters give rise to contrast modifications of the same magnitude. Few simulated images are shown in Fig. 6 for δ = 0.06 nm (other values were also considered, from 0.04 to 0.10 nm, not shown here). Fig. 6a–c illustrates the effect of changing the defect position h_d while keeping all other parameters at the same values. The changes of contrast at the core of the defect are obvious. Fig. 6d can be compared to Fig. 6b to evaluate the influence of the defect thickness t_d on the contrast. The influence of a slight modification of the total thickness t_s is visible by comparing Fig. 6d and e. At last Fig. 6e and f shows the effect of a drastic change of the defocus value for the very same model sample.

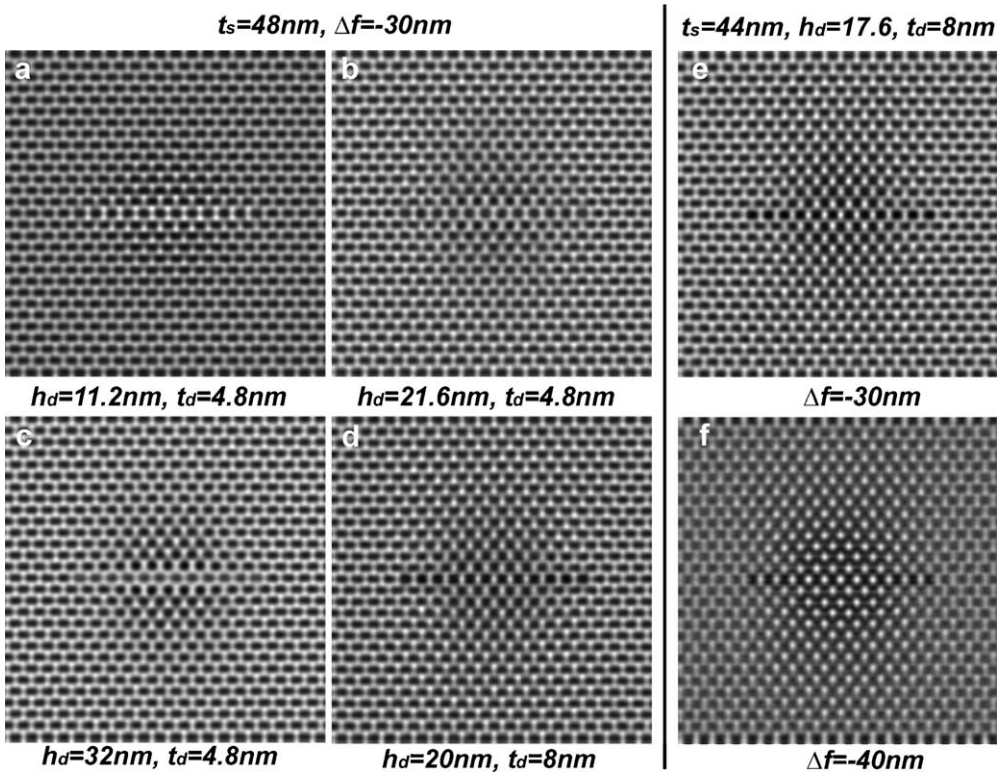

Fig. 6. (a)–(c) Multislice simulations of defects (t_d = 4.8 nm and t_d = 8 nm) located at different depth h_d along the electron beam path and at given t_s = 48 nm and Δf = −30 nm. (d) Simulated image showing the influence of the defect thickness t_d, to be compared with image (b) above. (e) and (f) Example of the influence of the defocus Δf on the contrast at the core of the defect located at h_d = 17.6 nm. The comparison between (d) and (e) shows the change in contrast at the core of the defect for a variation of the total thickness t_s (the core contrast is brighter in (e)).

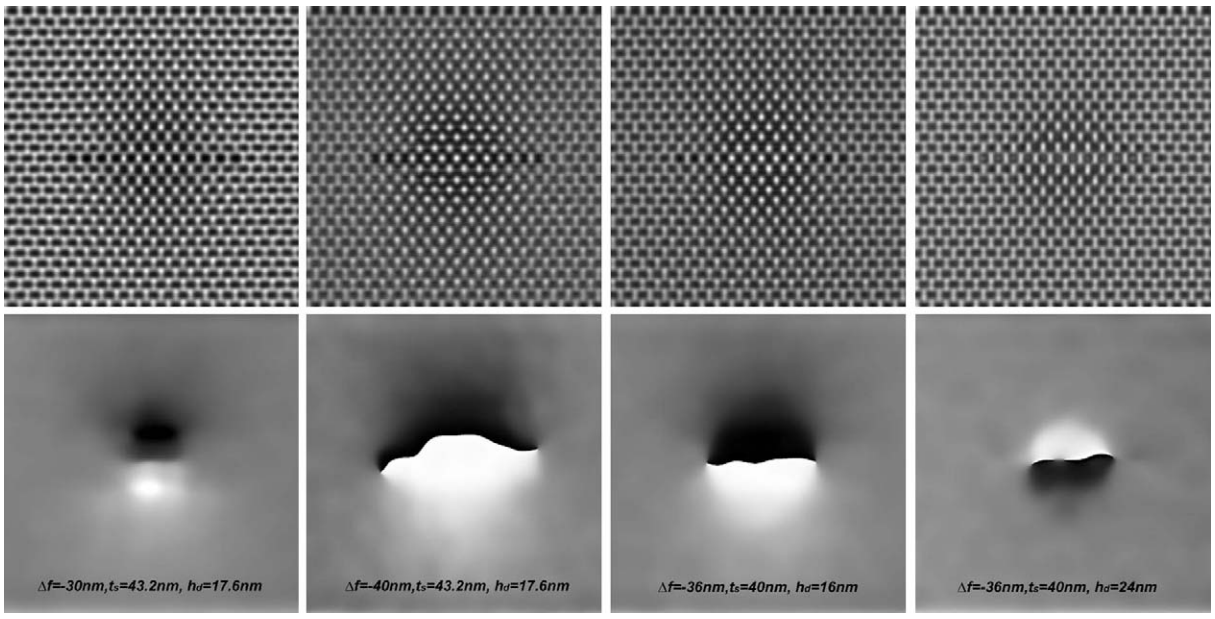

Fig. 7. Phase shift contrast variations for the very same defect (t_d = 8 nm, δ = 0.06 nm) for various parameters. Under specific conditions, the (0 0 2) phase shift contrast might be reversed (bottom right image), which would suggest a kind of vacancy loop (see Fig. 3g).

In order to limit the number of parameters and after several fruitless trials, we fixed the thickness of the defect considered for image simulation (t_d = 8 nm). This choice is supported by the fact that this value corresponds to the average size of the nanoplatelets observed in our experiment. Then the value of h_d was optimized. Fine tuning of t_s and Δf around the values previously determined was also performed to further improve the contrast matching. We point out that the use of an automated matching method could not be foreseen as the contrast variations as a function of these parameters are far from being linear or predictable. From these simulations, we thus conclude that the exclusive use of image matching cannot lead to a unique solution; too many parameters, responsible for similar effects (modification of the dumbbell-like contrast, brightness variations, ...), being involved in the calculations. Another point limiting the accuracy of the method is the influence of the so-called "Stobbs factor" which makes the comparison of absolute intensities relatively tricky (Hÿtch and Stobbs, 1994). Coupled to DFT calculations, such simulations can however be used to address some issues about the symmetry of the core defect configuration (David et al., 2009). A deeper analysis of the contrast would imply the consideration of several effects (Boothroyd and Dunin-Borkowski, 2004): phonon scattering (sample thickness was estimated to be greater than 20 nm) and scattering from a residual amorphous surface layer which could be partially at the origin of this lack of contrast. The influence of the MTF (modulation transfer function) of the detector (film/scanner or CCD) which has also recently been shown to be important (Thust, 2009), should be considered for a fully quantitative analysis of the contrast, but is out of the scope of our study.

It is thus not possible to determine the actual δ value with a high accuracy by a simple image matching method, variations of δ leading also to changes of brightness of the atomic columns located at the core of the defect and to shifts and variations of the dumbbell contrast. For instance, in Fig. 6f, the dumbbell-like contrast vanishes over a wide part of the image. Nevertheless such simulations can be used as input data to be processed via the GPA method in order to interpret the phase image shown in Fig. 3c and to shed light on the peculiar features reported above. The GPA method being very weakly sensitive to the absolute contrast value, we have compared the experimental data with simulated ones without applying any processing (MTF deconvolution) to the experimental micrographs.

Fig. 7 shows a set of simulated images together with their associated (0 0 2) phase shift images. The geometrical parameters of the defect have been set to t_d = 8 nm, δ = 0.06 nm for all images. This corresponds to the best match between experimental and simulated images, and also confirmed by DFT calculations (David et al., 2009). Then the influence of h_d, Δf or t_s on the phase image can be evaluated. Drastically different phase shift images are obtained: the maximum phase shift varies in both position and amplitude. Moreover, depending on the position of the defect in the sample, the phase shift might reverse from the actual one. This peculiar behaviour is attributed to a subtle interplay between the phase changes of the considered reflection (0 0 2) with the thickness of the sample and to the occurrence of strain variations along the sample thickness. One can also notice that the size of the defect also seems to vary, although it is actually the same in all models. These results prove that the interpretation of the HRTEM contrast for embedded defects should not be done without image simulation. Thus it appears tricky to get quantitative information from HRTEM images of such defects even in a qualitative manner.

Nevertheless, as seen in Fig. 8, the trial and error method described in the previous section might lead not only to a good match between experimental images and simulated ones, but also to a high level of similarity between the associated phase images. The amplitude of the phase shift obtained from the simulation is consistent with the experimental data, the position of the maxima as well. The maximum phase shift corresponds to an apparent lattice displacement of 0.07 nm located about 3 nm away from the core of the nanoplatelet on both images (the input strain being 0.06 nm at the core of the defect). The uniqueness of this solution is certainly questionable; however its comparison with atomic models determined by DFT calculations (David et al., 2009) allows converging to a reasonable set of geometrical parameters describing the nanoplatelet. More precisely, we can state that such platelets are surrounded by a strain field that is in agreement with the presence of a filling gas which induces a compressive stress on the crystalline lattice.

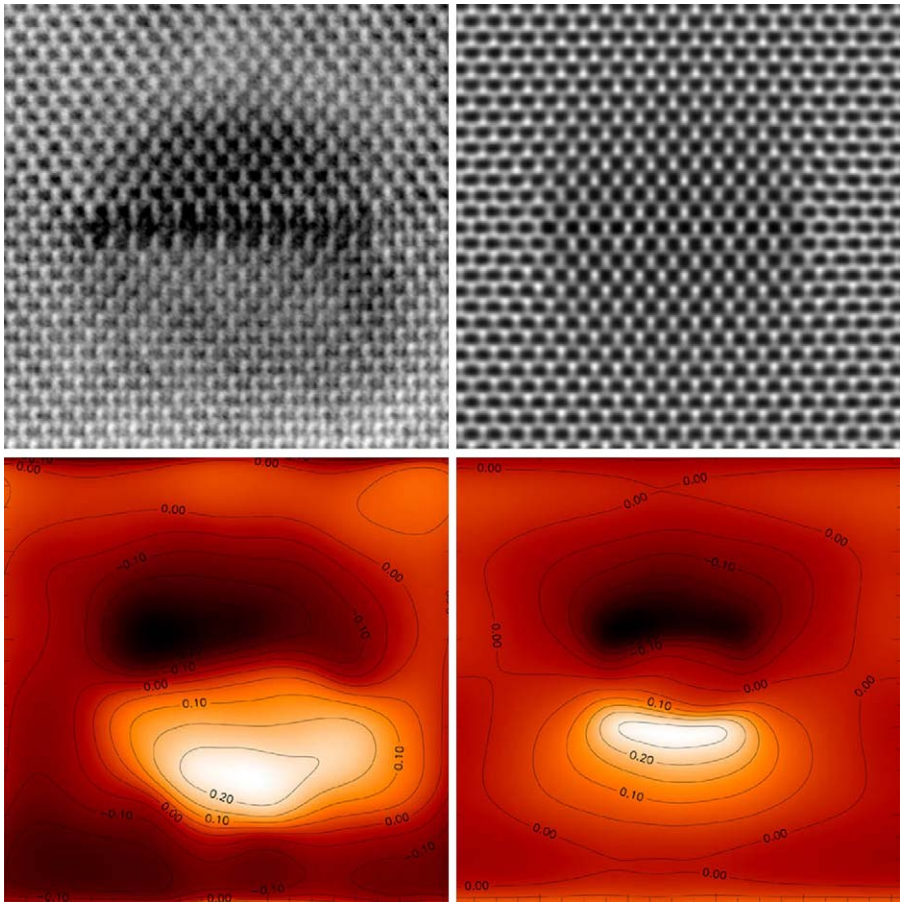

Fig. 8. Comparison between the experimental (left) and the simulated (right) images. HRTEM are displayed on top and (0 0 2) phase images at the bottom. The optimum matching simulated image was obtained for the following conditions: t_s = 44.8 nm, Δf = −28 nm, h_d = 18.4 nm, t_d = 8 nm and δ = 0.06 ± 0.01 nm.

5. Conclusion

We have conducted a set of experiments, image simulations and image processing in order to get quantitative insights from HRTEM images obtained on nanoplatelets created by hydrogen implantation into germanium. Our results strongly suggest that image simulations and analysis must be coupled in order to avoid misleading interpretation (even qualitative) of the phase images and to get a precise knowledge of the nanoplatelets structure. We particularly show that contrary to the case of threading defects, the analysis of a single HRTEM image of a nanoplatelet cannot lead to an accurate estimation of the strain field. The modelling of these defects by atomistic calculations coupled with strain field analysis of simulated pictures compared to the experimental ones must be envisaged. Such an approach can give a satisfactory level of matching between the phase images obtained from the simulated and experimental pictures. It leads to a good agreement of both the position and amplitude of the maximum displacement. One can thus describe with a relatively high level of confidence the strain field induced by the platelets, and by coupling with DFT calculations achieve a precise description of their atomic structure.

In this study, we have not precisely considered the impact of Fresnel fringes induced by the defocus conditions on the HRTEM contrast, which probably affects the actual intensity at the edge of the defect. Images obtained with aberration corrected microscopes could minimize this effect (which is tricky to quantify) and improve the accuracy of the measurements. Recent advances in HAADF HR-STEM imaging let also foresee the possibility of measuring the actual defect thickness and the amount of gas trapped in the platelet. We are confident in the idea that the method described here together with these technological improvements will lead to a better description of this class of defects or smaller ones (Barbot et al., 2008) within the next years.

References

Barbot, J.-F., Pailloux, F., David, M.-L., Pizzagalli, L., Oliviero, E., Lucas, G., 2008. Helium implanted gallium nitride evidence of gas-filled rod-shaped cavity formation along the c-axis. J. Appl. Phys. 104, 043526.

Barry, J.C., 1991. HRTEM of {1 0 0} platelets in natural 1aA diamond at 1.7 Å resolution: a defect structure refinement. Philos. Mag. A 64, 111–135.

Boothroyd, C.B., Dunin-Borkowski, R.E., 2004. The contribution of phonon scattering to high resolution images measured by off-axis electron holography. Ultramicroscopy 98, 115–133.

Bursill, L.A., Barry, J.C., Hudson, P.R.W., 1978. Fresnel diffraction at {1 0 0} platelets in diamond: an attempt at defect structure analysis by high-resolution (3 Å) phase-contrast microscopy. Philos. Mag. A 37, 789–812.

Bursill, L.A., Hutchinson, J.L., Sumida, J.L., Lang, A.R., 1981. Measurement of diamond lattice displacement by platelet defects with electron microscopic moiré patterns. Nature 292, 518–520.

Cherkashin, N., Hÿtch, M.J., Cristiano, F., Claverie, A., 2005. Structure determination of clusters formed in ultra-low energy high-dose implantated silicon. Solid State Phenom. 108-109, 303–308.

Cherns, D., Kaneko, K., Hovsepian, A., Lang, A., 1997. Measurement of the lattice displacement across {1 0 0} platelets in diamond by large-angle convergent-beam electron diffraction. Philos. Mag. A 75, 1553–1566.

David, M.-L., Pailloux, F., Babonneau, D., Drouet, M., Barbot, J.-F., Simoen, E., Claeys, C., 2007. The effect of the substrate temperature on extended defects created by hydrogen implantation in germanium. J. Appl. Phys. 102, 096101.

David, M.-L., Pizzagalli, L., Pailloux, F., Barbot, J.-F., 2009. Atomic scale structure of (0 0 1) hydrogen-induced platelets in germanium. Phys. Rev. Lett. 102, 155504.

Evans, T., Phaal, C., 1962. Imperfections in type I and type II diamonds. Proc. R. Soc. Lond. A 270, 538–552.

Evans, J.H., Van Veen, A., Casper, L.M., 1981. Formation of helium platelets in molybdenum. Nature 291, 310–312.

Fichtner, P.F.P., Kaschny, J.R., Behar, M., Yankov, R.A., Mücklich, A., Skorupa, W., 1999. The effects of the annealing temperature on the formation of helium-filled structures in silicon. Nucl. Inst. Methods Phys. Res. B 148, 329–333.

Goss, J.P., Coomer, B.J., Jones, R., Fall, C.J., Briddon, P.R., Öberg, S., 2003. Extended defects in diamond: the interstitial platelet. Phys. Rev. B 67, 165208.

Hayashi, S., Bruno, D., Goorsky, M.S., 2004. Temperature dependence of hydrogen-induced exfoliation of InP. Appl. Phys. Lett. 85, 236–238.

Humble, P., 1982. The structure and mechanism of formation of platelets in natural type Ia diamond. Proc. R. Soc. Lond. A 381, 65–81.

Humble, P., Mackenzie, J.K., Olsen, A., 1985. Platelet defects in natural diamond. I. Measurement of displacement. Philos. Mag. A 52, 506–521.

Hÿtch, M.J., Putaux, J.-L., Pénisson, J.-M., 2003. Nanoscale measurement of stress and strain by quantitative high-resolution electron microscopy. Nature 423, 270–273.

Hÿtch, M.J., Snoeck, E., Kilaas, R., 1998. Quantitative measurement of displacement and strain fields from HREM micrographs. Ultramicoscopy 74, 131–146.

Hÿtch, M.J., Stobbs, W.M., 1994. Quantitative comparison of high resolution TEM images with image simulations. Ultramicroscopy 53, 191–203.

Merkle, K.L., Csencsists, R., Rynes, K.L., Withrow, J.P., Stadelmann, P.A., 1998. J. Microsc. 190, 204–213.

Moutanabbir, O., Scholz, R., Senz, S., Gösele, U., Chicoine, M., Schiettekatte, F., Süsskraut, F., Krause-Rehberg, R., 2008. Microstructural evolution in H ion induced splitting of freestanding GaN. Appl. Phys. Lett. 93, 031916.

Muto, S., Takeda, S., Hirata, M., 1995. Hydrogen-induced platelets in silicon studied by transmission electron microscopy. Philos. Mag. A 72, 1057–1074.

Neethling, J.H., Snyman, H.C., Ball, C.A.B., 1988. Analysis of transmission electron microscopy images of hydrogen platelets in proton-bombarded GaAs. J. Appl. Phys. 63, 704–711.

Nomachi, T., Muto, S., Hirata, M., Kohno, H., Yamasaki, J., Takeda, S., 1997. Extended platelets on {1 1 1} in GaAs created by He-ion implantation followed by low temperature annealing. Appl. Phys. Lett. 71, 255–257.

Spence, J.C.H., 1982. Experimental High Resolution Microscopy. Oxford Univ. Press.

Stadelmann, P.A., 1987. EMS—a software package for electron diffraction analysis and HREM image simulation in materials science. Ultramicroscopy 21, 131–145., http://cimewww.epfl.ch/people/Stadelmann/jemsWebSite/jems.html.

Terreault, B., 2007. Hydrogen blistering of silicon: progress in fundamental understanding. Phys. Status Solidi A 204, 2129–2184.

Tersoff, J., 1989. Modeling solid-state chemistry: interatomic potentials for multicomponent systems. Phys. Rev. B 39, 5566.

Thust, A., 2009. High-resolution transmission electron microscopy on an absolute contrast scale. Phys. Rev. Lett. 102, 220801.